Optica Applicata XXXI, No. 2, 2001

Functional properties of dual-rail photonic image processor using comparator arrays

RYSZARD BUCZYŃSKI

Department of Applied Physics and Photonics, Faculty of Applied Sciences, Vrije Universiteit Brussel, Pleinlaan 2, B-1050 Brussels, Belgium.

TOMASZ SZOPLIK

Faculty of Physics, Warsaw University, ul. Pasteura 7, 02–093 Warsaw, Poland.

STANISŁAW JANKOWSKI

Faculty of Electronics, Warsaw University of Technology, ul. Nowowiejska 15/19, 00–665 Warsaw, Poland.

IRINA VERETENNICOFF, HUGO THIENPONT

Department of Applied Physics and Photonics, Faculty of Applied Sciences, Vrije Universiteit Brussel, Pleinlaan 2, B-1050 Brussels, Belgium.

We extend the description of a discrete-time cellular neural network, depicting the behaviour of both cellular and morphological processors, to any type of dual-rail processors. We show that a system with two arrays of differential pairs of transceivers can be treated as a two-layer cellular network and that it can perform morphological and rank order filter operations. As an illustration we built and tested a dual-rail processor composed of arrays of GaAs optical thyristor differential pairs and highlight experimental results on median filtering.

1. Introduction

Photonic techniques which combine optically implemented operations with electronic processing may lead to massively parallel image processing. In the latter, and in particular for local image processing, optical interconnections and local convolutions are of fundamental importance. Here the modification of an image structure is based on the evolutionary influence of the neighbourhood on each of its pixels. Since the early eighties different names have been given to local techniques such as morphological processing [1], optical-logic-array processing [2], [3], symbolic substitution [4], [5], cellular processing and cellular neural networks (CNN) [6]–[8]. As said above, the optical interconnects paradigm always plays an important role. By interconnects we mean all the possible ways of exchanging information between the pixels of an image to be processed. Here, the most interesting interconnections are those between a pixel and its neighbourhood. Typically, the neighbourhood operation is realised through imaging with an adequately chosen point spread function that defines the size of the local convolution.

It took more than a decade to recognize and analyse all the operations and functions necessary for non-linear parallel image processing. Most of the early processors were implemented as simple shadow casting correlators usually composed of spatial light modulators based on nematic liquid crystals [3], [5], [9]–[15]. Only recently, photonic processor demonstrators were constructed using differential-pair optical-thyristor arrays [16], [17], arrays of vertical-cavity surface-emitting lasers (VCSELs) [18] or multiple-quantum-well (MQW) devices [19]. Today, arrays of VCSELs and GaAs MQW devices are combined with complementary metal-oxide-semiconductor (CMOS) circuitry using flip-chip bonding techniques to form smart-pixel structures [20]–[23]. The main advantage of these novel devices is the possibility of truly parallel pixel-oriented processing where convolution, transfer, data acquisition and storage are performed in parallel.

These new perspectives for free-space photonic switching nurture research on architectures and programmable space-variant interconnects [24], [25] for a specific parallel photonic image processing. The question of what operations should be performed either optically or electronically is still open. Most of the laboratories agree that optics offers advantages in performing parallel interconnects. A lot of work is also dedicated to reconfigurable parallel interconnects.

In this paper, we present a dual-rail architecture for a photonic cellular/morphological processor constructed with matrices of differential pairs of transceivers. In Section 2, we recall conventional descriptions of optical cellular processors. We show that the CNN formalism can be used to perform morphological and rank order filters. We then show in Section 3 that the dual-rail regime is advantageous in a photonic cellular processor where the output function of the CNN is implemented in a differential detector. In Section 4, we describe a demonstrator consisting of arrays of optical thyristor differential pairs made in GaAs technology. We show the benefits of introducing into optics another operation that is a hard clip threshold, important for the decomposition of grey-scale images into a series of binary slices. The photonic processor functionality is illustrated with experimental results on median filtering presented in Section 5.

2. Optical cellular/morphological processors

Usually, the output state of each cell y_{ij} of a two-dimensional cellular processor array, as schematically shown in Fig. 1, can be described by the following general expression [6]:

$$y_{ij} = F_{ij}\,(u_{ij}, u_{kl} : u_{kl} \in V_{ij})$$

where u_{ij} and u_{kl} are the input states of the cell ij and the cells kl from its neighbourhood V_{ij}. Each input and output state is binary and may correspond to two values of an intensity transmission coefficient, to two polarization states, or to two values of an intensity reflection coefficient.

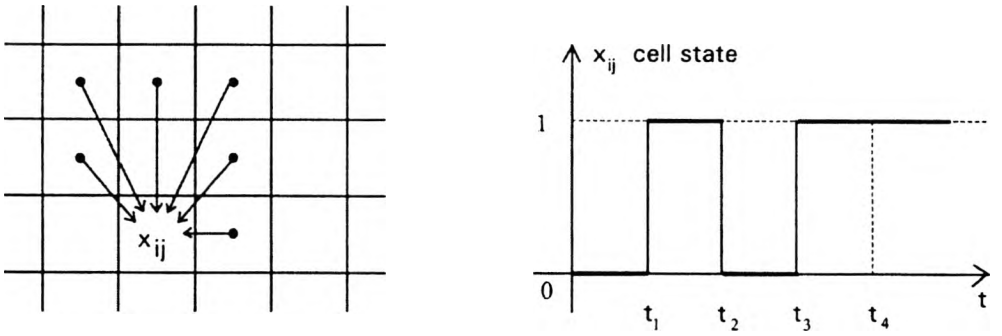

Fig. 1. Optical cellular processor with an active neighborhood of x_{ij} image cell.

A binary optical cellular processor is characterized by the following five properties:

1. The new values of the pixels are calculated synchronously at discrete clock times.

2. The neighbourhood V_{ij}, which determines the interconnection pattern in the image plane is identical for all ij values.

3. Its evolution function F_{ij} is also space invariant for local image processing realised in a single-instruction multiple-data case.

4. Both the neighbourhood V_{ij} and the evolution function F_{ij} may be programmable. They can therefore be a function of time.

5. Output and input values of an image cell (called y_{ij} and u_{ij}, respectively) accept only binary values in the stable state of the network.

2.1. CNN state and output equations

In the classical theory of CNNs [7], the evolution of every cell is described by the differential state equation

$$\frac{\mathrm{d}x_{ij}}{\mathrm{d}t} = -\frac{x_{ij}}{\tau} + \sum_{k=-r}^{r}\sum_{l=-r}^{r} A_{kl}y_{i+k,j+l} + \sum_{k=-r}^{r}\sum_{l=-r}^{r} B_{kl}u_{i+k,j+l} + I \tag{2}$$

where u_{ij} and y_{kl} are the input and output states of the cell ij, respectively; x_{ij} denotes its internal state which accepts an arbitrary real value, for example, of intensity.

The output equation usually takes the form of a piecewise linear function

$$y_{ij} = f(x_{ij}) = \frac{1}{2}\left(|x_{ij}+1| - |x_{ij}-1|\right). \tag{3}$$

The state and output equations together are a special case of Eq. (1). The meaning of Eqs. (2) and (3) is illustrated with Fig. 2, which shows the scheme of a single cell processing. The dynamics of the network is imbedded in the four parameters that influence the internal state of the cell x_{ij}:

1. The time constant τ of every cell. It may be interpreted as the time constant of the input circuit of a given cell in a typical electronic implementation [7].

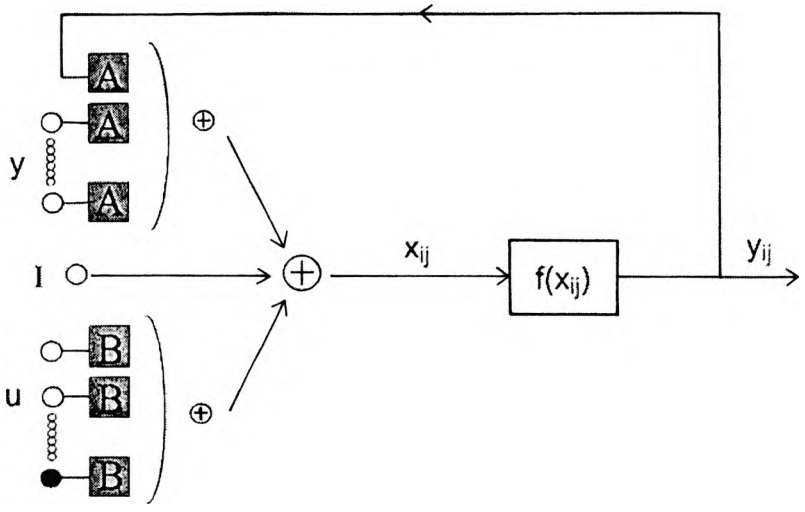

Fig. 2. The scheme of a single cell processing.

2. The output signals $y_{i+k,\,j+l}$ from the neighbourhood cells are taken into account with the weights gi en b a feedback operator $A_{i,\,j,\,i+k,\,j+l}$.

3. The input signals $u_{i+k\,j+l}$ from the neighbourhood cells are taken into account with the weights given by a control operator $B_{i,\,j,\,i+k,\,j+l}$.

4. The polarization signal I. It acts as an offset signal which allows a choice of the network operation.

It follows from the above description that the cell state x_{ij} as well as the output signal y_{ij} are continuous variables. However, if the stability conditions are satisfied, then the output signal of every cell tends to either 1 or -1 after a transient time. If the output function $f(x_{ij})$ takes the form of a threshold, then the state evolution of a cellular neural network does not undergo continuous changes. In that case, the new binary states are calculated at every discrete clock cycle. Then, the state and output equations can be written as

$$x_{ij}(n+1) = \sum_{k=-r}^{r} \sum_{l=-r}^{r} A_{kl}\, y_{i+k,j+l}\,(n) + \sum_{k=-r}^{r} \sum_{l=-r}^{r} B_{kl}\, u_{i+k,j+l}\,(n) + I\,, \tag{4}$$

$$y_{ij}(n+1) = \operatorname{sgn}(x_{ij}(n+1)) = \begin{cases} 1, & x_{ij} \geq 0 \\ -1, & x_{ij} < 0 \end{cases}, \tag{5}$$

and the network is called a discrete-time CNN (DT CNN) [26]. In principle, these discrete-time equations are suited for optical implementations, where iterations n and $n+1$ are separated in time by a constant τ corresponding to integration time of optical detectors used in the system. However, it is difficult to build an optical system able to

calculate a result of Eq. (4) equal to a natural number and threshold it on an arbitrary zero level according to Eq. (5). Nevertheless, these equations are useful for sequential image processing with feedforward and feedback operations, which is explained below.

2.2. Morphological operations and rank order filtering in DT CNN

It can be shown that the basic morphological operations erosion and dilation can be expressed in the DT CNN formalism under the condition that the task of the morphological structuring element is performed by the CNN control (or feedforward) operator B and the polarization signal I, while the feedback operator A is taken equal to zero. The value of the polarization signal depends on the number of non-zero elements in the neighbourhood and is equal:

$$I = -\sum_{k=-r}^{r}\sum_{l=-r}^{r} B_{kl} + 1 \text{ for erosion and } I = \sum_{k=-r}^{r}\sum_{l=-r}^{r} B_{kl} - 1 \text{ for dilation.}$$

For example, the nearest neighbourhood CNN template with a radius $r = 1$ for the morphological erosion and dilation can be presented as [27]:

$$\text{erosion: } A = \begin{bmatrix} 0 & 0 & 0 \\ 0 & 0 & 0 \\ 0 & 0 & 0 \end{bmatrix}, \quad B = \begin{bmatrix} 1 & 1 & 1 \\ 1 & 1 & 1 \\ 1 & 1 & 1 \end{bmatrix}, \quad I = -8,$$

$$\text{dilation: } A = \begin{bmatrix} 0 & 0 & 0 \\ 0 & 0 & 0 \\ 0 & 0 & 0 \end{bmatrix}, \quad B = \begin{bmatrix} 1 & 1 & 1 \\ 1 & 1 & 1 \\ 1 & 1 & 1 \end{bmatrix}, \quad I = 8, \tag{6}$$

Besides morphological operations also all rank order filters can be realized in the DT CNN formalism. In this case, the neighbourhood is defined by the control operator B, while the filter type is determined by selecting the proper polarisation signal. The value of the polarisation I_x to perform x-th rank order filtering is given by the following equation:

$$I_x = 2x - \sum_{k=-r}^{r}\sum_{l=-r}^{r} B_{kl} - 1. \tag{7}$$

For example, the CNN template for median filtering ($x = 5$) is as follows:

$$A = \begin{bmatrix} 0 & 0 & 0 \\ 0 & 0 & 0 \\ 0 & 0 & 0 \end{bmatrix}, \quad B = \begin{bmatrix} 1 & 1 & 1 \\ 1 & 1 & 1 \\ 1 & 1 & 1 \end{bmatrix}, \quad I = 0. \tag{8}$$

Simple morphological filters are realized as a sequence of the two basic morphological operations, erosion and dilation. In this way, an erosion operation

followed by a dilation yields the opening of an image, while dilation followed by erosion performs the closing of an image. However, to implement these filtering operations in practical system a kind of feedback in the system is needed. This can be realised in a two-layered neural network where each layer is represented by an array of photonic transceivers. In the first step, an image from the first layer is fed forward to the second one according to Eqs. (4) and (5). While in the second step, the information contained in the second layer is fed back to the first one. Thus, for an opening operation the set of control (feedforward), feedback and polarization operators are as follows:

$$\text{opening}\begin{cases}\text{erosion:} \quad A = \begin{bmatrix}0&0&0\\0&0&0\\0&0&0\end{bmatrix}, \quad B = \begin{bmatrix}1&1&1\\1&1&1\\1&1&1\end{bmatrix}, \quad I = -8, \\ \text{dilation:} \quad A = \begin{bmatrix}1&1&1\\1&1&1\\1&1&1\end{bmatrix}, \quad B = \begin{bmatrix}0&0&0\\0&0&0\\0&0&0\end{bmatrix}, \quad I = 8.\end{cases} \tag{9}$$

These operators correspond to the sequential solution of the state and output Eqs. (4) and (5). In the case of morphological filters the second operation is interpreted differently than a single morphological operation in terms of the DT CNN description. Since the second operation is performed in feedback, the feedback operator defines the neighbourhood while the control operator is equal to zero. However, from the point of view of implementation both the control operator (that performs feedforward operations) and feedback operator are realised by the same element.

3. Dual-rail processor

The DT CNN output Eq. (5) says that the output function of a network is binary and boils down to the sign of the state of a cell. The best way to realise this operation in optics is to use dual rail arithmetics [27]. Thus, instead of thresholding the result of Eq. (4) on an arbitrary zero level we compare its positive and negative parts. Our choice is justified since the differential-pair optical-thyristor arrays can be used as comparator devices [28]–[30]. Equations (4) and (5) are divided into a positive and a negative part. The state and output equations of DT CNN using dual rail notation can be written as:

$$x_{ij}^{+}(n+1) = \sum_{k=-r}^{r}\sum_{l=-r}^{r} A_{i,j,i+k,j+l}^{+} y_{i+k,j+l}^{+}(n)$$

$$+ \sum_{k=-r}^{r}\sum_{l=-r}^{r} B_{i,j,i+k,j+l}^{+} u_{i+k,j+l}^{+}(n) + I^{+},$$

$$x_{ij}^{-}(n+1) = \sum_{k=-r}^{r} \sum_{l=-r}^{r} A_{i,j,i+k,j+l}^{-} y_{i+k,j+l}^{-}(n) + \sum_{k=-r}^{r} \sum_{l=-r}^{r} B_{i,j,i+k,j+l}^{-} u_{i+k,j+l}^{-}(n) + I^{-},$$

$$y_{ij}^{+}(n+1) = \begin{cases} 1 & x_{ij}^{+}(n+1) - x_{ij}^{-}(n+1) \geq 0 \\ 0 & x_{ij}^{+}(n+1) - x_{ij}^{-}(n+1) < 0 \end{cases},$$

$$y_{ij}(n+1) = \begin{cases} 1 & x_{ij}^{+}(n+1) - x_{ij}^{-}(n+1) < 0 \\ 0 & x_{ij}^{+}(n+1) - x_{ij}^{-}(n+1) \geq 0 \end{cases} \tag{10}$$

where: $I = I^{+} - I^{-}$

$$u_{ij}^{+}(n) = \begin{cases} 1 & u_{ij} = 1 \\ 0 & u_{ij} = -1 \end{cases},$$

$$u_{ij}^{-}(n) = \begin{cases} 1 & u_{ij} = -1 \\ 0 & u_{ij} = 1 \end{cases},$$

$$y_{ij}(n+1) = \operatorname{sgn}(x_{ij}^{+}(n+1) + x_{ij}^{-}(n+1)) = \begin{cases} 1 & x_{ij}^{+}(n+1) - x_{ij}^{-}(n+1) \geq 0 \\ -1 & x_{ij}^{+}(n+1) - x_{ij}^{-}(n+1) < 0 \end{cases},$$

All parameters indicated by "+" denote positive part of the parameters, while all parameters indicated by "–" denote negative part of the parameters. For example, I^{+} represents a positive part of a polarization and I^{-} – a negative part of a polarization.

The dual-rail configuration has interesting properties from the point of view of its implementation with photonic components:

1. A CNN output function is reduced to a comparison between the positive and negative parts of the state of cell signals. Therefore comparator devices can be used to perform this operation. As comparators we can take any kind of differential detectors combined with a pair of emitters or transceivers: all the positive signals from the neighbourhood (denoted by "+") are directed to one of the detectors in a pair, while all the negative signals from the neighbourhood (denoted by "–") are directed to the other.

2. No additional electronics is necessary to perform morphological operation or rank-order filtering (no flip-chip bonding).

3. The local neighbourhood of any pixel is the same for positive and negative signals. This means that the same shift-invariant diffractive fan-out element can be used to generate local interconnection between a pixel and its neighbourhood.

4. Morphological filters can be performed in the dual-rail system in a two layer cellular network, in which every layer consists of an array of comparators.

A conversion of both the state and output equations of DT CNN to the dual arithmetic representation requires the template notation to be changed. The templates for the nearest neighbourhood erosion and dilation can be defined as follows:

$$\text{erosion:}\quad A^{+} = \begin{bmatrix} 0 & 0 & 0 \\ 0 & 0 & 0 \\ 0 & 0 & 0 \end{bmatrix}, \quad B^{+} = \begin{bmatrix} 1 & 1 & 1 \\ 1 & 1 & 1 \\ 1 & 1 & 1 \end{bmatrix}, \quad I^{+} = 0,$$

$$A^{-} = \begin{bmatrix} 0 & 0 & 0 \\ 0 & 0 & 0 \\ 0 & 0 & 0 \end{bmatrix}, \quad B^{-} = \begin{bmatrix} 1 & 1 & 1 \\ 1 & 1 & 1 \\ 1 & 1 & 1 \end{bmatrix}, \quad I^{-} = 8, \tag{11}$$

$$\text{dilation:}\quad A^{+} = \begin{bmatrix} 0 & 0 & 0 \\ 0 & 0 & 0 \\ 0 & 0 & 0 \end{bmatrix}, \quad B^{+} = \begin{bmatrix} 1 & 1 & 1 \\ 1 & 1 & 1 \\ 1 & 1 & 1 \end{bmatrix}, \quad I^{+} = 8,$$

$$A^{-} = \begin{bmatrix} 0 & 0 & 0 \\ 0 & 0 & 0 \\ 0 & 0 & 0 \end{bmatrix}, \quad B^{-} = \begin{bmatrix} 1 & 1 & 1 \\ 1 & 1 & 1 \\ 1 & 1 & 1 \end{bmatrix}, \quad I^{-} = 0. \tag{12}$$

4. Demonstrator dual-rail cellular/morphological processor

We have built a proof-of-principle demonstrator of dual-rail cellular morphological processing. As comparator devices we used differential pairs of optical thyristors. The latter are bistable photonic transceiver elements, which are usually implemented as PnpN double heterostructures in the GaAs/AlGaAs material system [28]–[30]. In the off-state they have a high impedance and work as detectors. When the voltage across them is raised above a break-over level (V_{BR} = 5 V) the two elements compete for photo-induced current. The break-over voltage can also be reduced due to the influence of external illumination, making them optically sensitive. The thyristor that has received more optical energy will win this competition and will switch "on" while its neighbour remains in the "off" state. The sensitivity of these devices is considerably enhanced when they form a differential pair and work as an optical comparator.

Switching energy of the thyristor sufficient to induce the comparator asymmetry is low and amounts to 15 aJ/μm^2 of the device area. After switching, the thyristors are reset with application of −5 V reset voltage which completely depletes them of charge carriers in less than 5 ns.

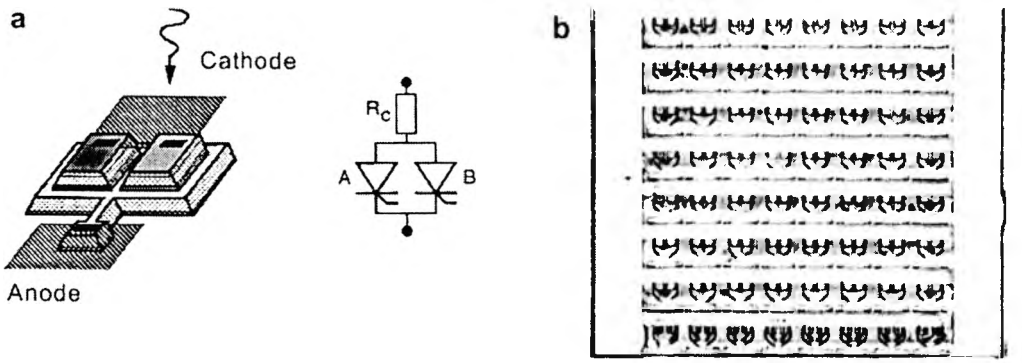

Fig. 3. Differential pair of optical thyristors and its electrical scheme (**a**), an 8×8 array of comparators (**b**).

Figure 3**a** shows schemes of one differential pair of optical thyristors and its electrical circuit. Figure3**b** presents an 8×8 array of comparators of the type that was used in the experiment. The pitch of the pairs is 95×100 μm, the centre separation of two elements in a pair is 45 μm and the size of each thyristor active optical window is 30×30 μm.

The experimental system consists of four parts as schematically shown in Fig. 4:

1) the external input module,
2) the transcription module,
3) the reference signal module,
4) the processing module.

The external input module delivers a binary image to the comparator array T1 in the transcription module by means of a spatial light modulator (SLM) and an imaging optical system. We use a nematic liquid crystal SLM with 640×480 pixels, 24×24 μm pixel size. The SLM is placed in the focal plane of the lens L1. An image is downloaded from a PC computer to the SLM by a monitor port. Since the pitch of the SLM pixels does not match that of the comparator, an array of 4×4 SLM pixels is used to address one of the two detectors in each pair of the comparator. The SLM display works in an amplitude mode and is illuminated by a halogen lamp with a 30 nm bandwidth obtained with a red filter with a central wavelength of 680 nm.

The image signals in dual rail regime from the comparator array T1 is modified by processing diffractive grating G2 and addresses processing comparator array T2. Diffractive grating G2 plays a role of control operator to obtain the desired interconnection pattern between the transcription T1 and the processing T2 planes. After comparison operation in T2 array output signals are directed into output (in case

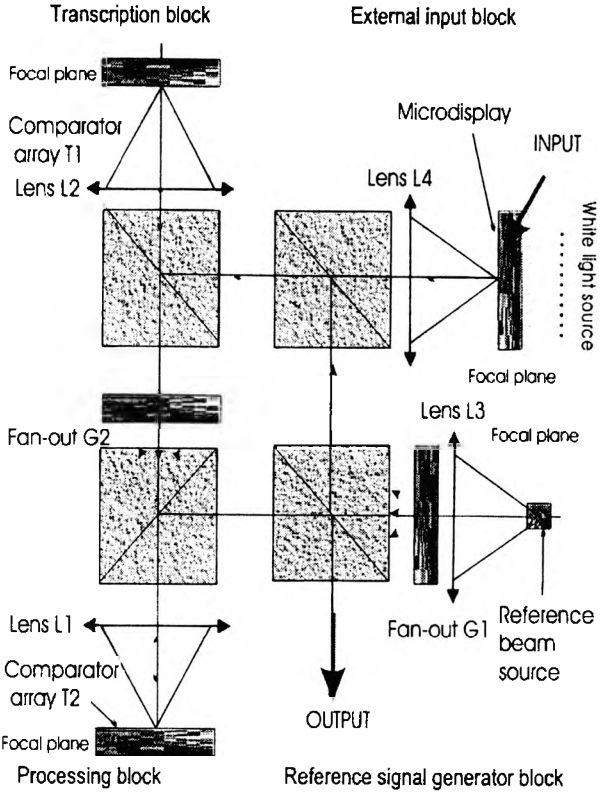

Fig. 4. Architecture of the cellular/morphological processor.

of erosion, dilation or rank order filter performance) or address T1 array in the next iteration (in case of morphological filter performance).

In the reference signal generator module two independently controlled VCSELs are used to illuminate the diffractive grating G1 and generate a beam array. The grating with a fan-out 1 to 64 was used. The beams generated by one of the VCSELs and diffractive grating G1 address either all the thyristors of the differential pair array T2 either representing one or zero. The values of the optical reference signals are controlled by drive current supplied to the VCSELs.

The optical imaging system used in this demonstrator consists of four GRIN lenses, each with a length of 31.9 mm, a diameter of 5 mm and a pitch of 0.20, permitting 4.5 mm working distance between the device arrays and the lenses. The field of view of the optical system is 2.5×2.5 mm. Three 50/50 beam-splitters placed in the centre of the optical system allow input of data to the device planes and output of data to a CCD camera. The total size of the whole optical system is about 10 cm by 10 cm [31].

The cellular/morphological processor shown in Fig. 4 can also work as a thresholder. In this case, an input signal from the external input block arrives to the comparator array T1 in the transcription block and is compared with the reference

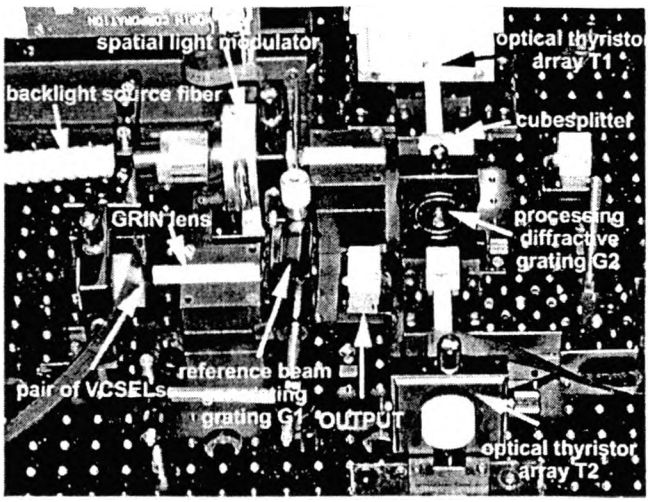

Fig. 5. Photo of the demonstrator system constructed for cellular/morphological image processing.

beam from the reference signal generator block. A binary slice of the input image may then be processed in the interaction between comparator arrays T1 and T2. Detailed description of the thresholder was published elsewhere [32].

The photo of the demonstrator system constructed for cellular/morphological image processing is presented in Fig. 5.

5. Experimental result: median filter

To show the functionality of the CNN we present experimental results of median filtering. Three different diffractive gratings, which perform a fan-out 1 to 3, 1 to 9 and 1 to 5 are placed between thyristor arrays T1 and T2. The median filtering is performed for 1D and 2D nearest neighbourhoods. We obtained good results using 63 pixels of 64 pixel array. One element of the transceivers arrays marked with a cross was defected.

In each cell of the array two thyristors are connected together and they work as a comparator. Only one of them emits light, namely the one which gets the most optical energy. This means that if there are more zero signals than one signals in the neighbourhood, then the thyristor representing zero will emit light. In the case of a surplus of one-valued signals the thyristor representing a logic one will emit light. For binary input signals this operation is equivalent to median filtering. Experimental results are presented in Fig. 6.

In the experiment the median filtering of several input images was performed. The median filtering was performed at 100 Hz. The reason for such a low speed is the low energy transfer between the two thyristor arrays, which is limited by the low emission efficiency of the optical thyristors themselves. Moreover, every positive and negative beam is divided into an array of beams during an image transfer between the

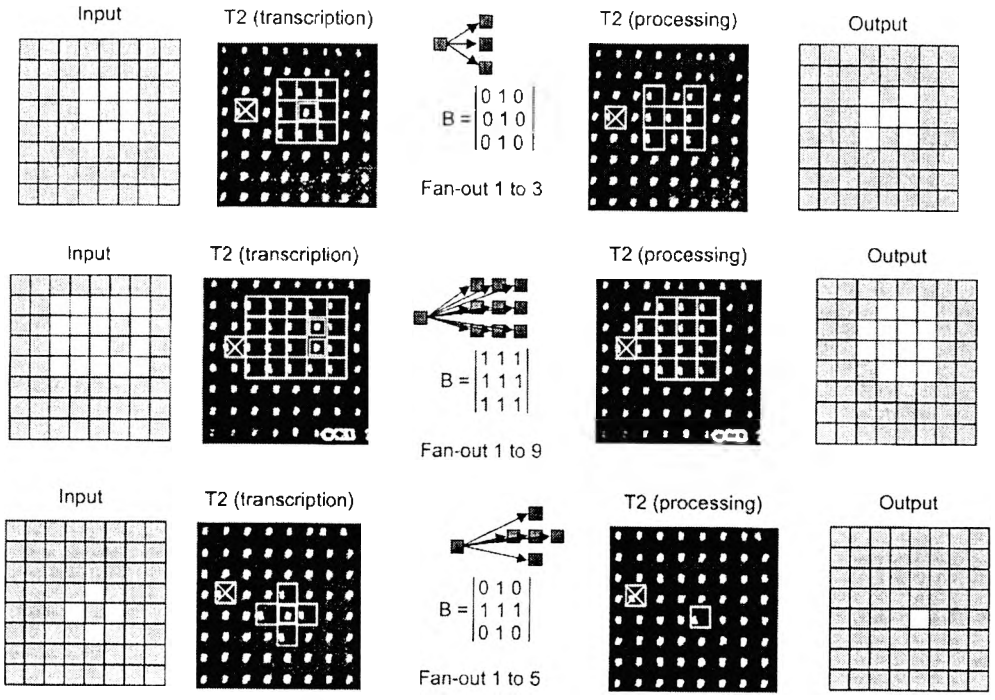

Fig. 6. Results of median filtering.

comparator arrays T1 and T2. For proper performance of differential pairs a certain minimum energy difference between thyristors in the pair has to be ensured and therefore the time of energy transfer has to be longer than in the case of simple data transcription without fanning-out.

6. Conclusions

In this paper, we discussed the functionality of a dual-rail photonic processor composed of two comparator layers which communicate forward and backward. The processor allows local image processing within neighbourhoods in both planes defined by the diffractive fan-out element. It is shown that the processor has the properties of both a DT CNN and a morphological processor. We treat sequential morphological filters as folded operations, which can be considered as stepwise feedforward and feedback.

In the processor, the arrays of integrated optical detectors and emitters are arranged in differential pairs. Its comparator regime of work is described with dual-rail DT CNN state and output equations. The theoretical considerations are illustrated with the demonstrator built of differential-pair optical-thyristor arrays. Its functionality is demonstrated with experimental results of median filtering. Apart from the property of morphological and cellular processing the demonstrator has the ability of grey scale

image thresholding on levels controlled by a reference beam originating from a current driven VCSEL.

The dual rail working regime of the system, where state and output equations accept binarized values allows parallel optical-digital image processing.

References

[1] SERRA J., *Image Analysis and Mathematical Morphology*, Academic, New York, 1982.

[2] CHAVEL P., FORCHHEIMER R., JENKINS B. K., *et al.*, *Architectures for sequential optical logic processor*, [In] *Proc. Tenth International Optical Computing Conf.*, MIT University Press, Cambridge, Mass., 1983, pp. 6–12.

[3] TANIDA J., ICHIOKA Y., J. Opt. Soc. Am. A **2** (1985), 1245.

[4] HUANG A., *Parallel algorithms for optical digital computers*,[In] *Proc. Tenth International Optical Computing Conf.*, MIT University Press, Cambridge, Mass., 1983, pp. 13–17.

[5] BRENNER K.-H., HUANG A., STREIBL N., Appl. Opt. **25** (1986), 3054.

[6] TABOURY J., WANG J. M., CHAVEL P., *et al.*, Appl. Opt. **27** (1988), 1643.

[7] CHUA L. O., YANG L., IEEE Trans. Circuits Syst. **35** (1988), 1257.

[8] PEIFFER W., THIENPONT H., Opt. Comput. Process. **3** (1993), 73.

[9] SZOPLIK T., GARCIA J., FERREIRA C., Appl. Opt. **34** (1995), 267.

[10] GEDZIOROWSKI M., GARCIA J., Opt. Commun. **119** (1995), 207.

[11] ICHIOKA Y., IWAKI T, MATSUOKA K., Proc. IEEE **84** (1996), 694.

[12] YATAGAI T., KAWAI S., HUANG H., Proc. IEEE **84** (1996), 828.

[13] KONISHI T., TANIGUCHI S., TANIDA J., ICHIOKA Y., Appl. Opt. **35** (1996), 1234.

[14] SZOPLIK T., [Ed.], *Morphological Image Processing: Principles and Optoelectronic Implementations*, SPIE Milestone Series MS **127**, SPIE, Bellingham, 1996.

[15] HUANG G., JIN G., WU M., YAN Y., Appl. Opt. **36** (1997), 5675.

[16] PASSON C., MOISEL J., MCARDLE N., *et al.*, Appl. Opt. **35** (1996), 1205.

[17] KIRK A., GOULET A., THIENPONT H., *et al.*, Appl. Opt. **25** (1997), 3070.

[18] STRZELECKA E. M., LOUDERBACK D. A., THIBEAULT B. J., *et al.*, Appl. Opt. **37** (1998), 2911.

[19] KOPPA P., CHAVEL P., OUDAR J. L., *et al.*, Appl. Opt. **36** (1997), 5706.

[20] GOOSEN K. W., WALKER J. A., D'ASARO L. A., *et al.*, IEEE Photon. Technol. Lett. **7** (1995), 360.

[21] WALKER A. C., YANG T.-Y., GOURLAY J., *et al.*, Appl. Opt. **37** (1998), 2822.

[22] KIM J., GUILFOYLE P. S., STONE R. V., *et al.*, Proc. SPIE **4089** (2000), 721.

[23] CHOQUETTE K. D., KENT D., HIETALA V. M., *et al.*, Proc. SPIE **4089** (2000), 704.

[24] MICHAEL N., ARRATHOON R., Appl. Opt. **36** (1997), 1718.

[25] HUANG C.-C., JENKINS B. K., KUZNIA C. B., Appl. Opt. **37** (1998), 889.

[26] HARRER H., NOSSEK J. A., Internat. J. Circ. Theory Appl. **20** (1992), 453.

[27] BUCZYŃSKI R., THIENPONT H., JANKOWSKI S., *et al.*, *Programmable CNN based on optical thyristors for early image processing*, [In] *Proc. Fifth IEEE Internat. Workshop on Cellular Neural Networks and Their Applications*, IEEE Catalog 98TH8359, London, 1998, pp. 259–264.

[28] PANKOVE J. I., HAYES R., MAJERFELD A., *et al.*, Proc. SPIE **963** (1988), 191.

[29] HEREMANS P., KUIJK M., VOUNCKX R., BORGHS G., Appl. Phys. Lett. **65** (1994), 19.

[30] KNUPFER B., KUIJK M., HEREMANS P., *et al.*, Electron. Lett. **31** (1995), 485.

[31] BUCZYŃSKI R., PhD Thesis, Vrije Universiteit Brussel, 1999.

[32] BUCZYŃSKI R., BAUKENS V., SZOPLIK T., *et al.*, IEEE Photon. Technol. Lett. **11** (1999), 367.

Received November 20, 2000